Interface-driven noncollinear magnetic structure and phase transition of Fe thin films

Taizo Kawauchi,[1,*] Yoshio Miura,[2,3] Xiaowei Zhang,[4] and Katsuyuki Fukutani[1,†]

[1]*Institute of Industrial Science, The University of Tokyo, Komaba, Meguro-ku, Tokyo 153-8505, Japan*

[2]*Electrical Engineering and Electronics, Kyoto Institute of Technology, Matsugasaki Sakyo-ku, Kyoto 606-8585, Japan*

[3]*Center for Spintronics Research Network (CSRN), Graduate School of Engineering Science, Osaka University, Toyonaka 560-8531, Japan*

[4]*Institute of Materials Structure Science, High Energy Accelerator Research Organization, Oho, Tsukuba, Ibaraki 305-0801, Japan*

(Received 1 September 2016; revised manuscript received 8 December 2016; published 30 January 2017)

We investigate the magnetic structure and its temperature dependence of Fe thin films grown on MgO(001) and Al_2O_3(0001) surfaces by means of nuclear resonant x-ray scattering. By fabricating Fe films δ-doped with ^{57}Fe at the interface and middle of the film, depth-resolved analysis of the magnetic structure is performed. On MgO(001), the magnetization is dominantly out-of-plane at the interface, whereas it is mainly in-plane at the middle of the film, indicating that the Fe film has a noncollinear magnetic structure. On Al_2O_3(0001), on the other hand, the magnetization is mainly in-plane in the entire film. The noncollinear magnetic structure on MgO(001) is confirmed to be energetically stable with the aid of first-principles calculations. We also investigate the temperature dependence of the internal magnetic field in a depth-resolved way. The experimental data suggest the internal magnetic field at the interface is smaller than that of the middle of the film on both substrates, suggesting that the magnetic phase transition starts at the interface at a lower temperature than the entire film.

DOI: 10.1103/PhysRevB.95.014432

I. INTRODUCTION

The magnetic structure of magnetic thin films is of fundamental interest as well as practical importance for magnetic storage devices. When two magnetic materials are stacked in a layered structure, the two materials are exchange-coupled at the interface, which offers a new magnetic device [1]. Even when one of the materials is nonmagnetic, the symmetry breaking at the interface brings about the interface magnetocrystalline anisotropy through the spin-orbit interaction reflecting the modified crystal field. This often reveals changes in the easy magnetization direction of ultrathin magnetic films, which depends on the thickness, surface condition, and temperature [2]. When competing interactions are present, the magnetization is not necessarily uniform in the entire film, and a noncollinear magnetic structure might appear [3,4]. At surfaces and interfaces, the magnetic anisotropy due to the broken symmetry competes with the bulk magnetocrystalline anisotropy, which is expected to cause magnetic canting [4,5]. At surfaces or interfaces, furthermore, the exchange interaction and magnetic moment might be different from those in bulk [6], which possibly affects the temperature dependence of the magnetization. The effects of surfaces on the temperature dependence of magnetization are twofold: whereas modification of the spin-wave excitation affects the magnetization in a low-temperature region, changes in the exchange interaction and symmetry modify the critical phenomenon at high temperature. The latter has been intensively studied via molecular-field theory, Monte Carlo simulations, high-temperature series expansions, and renormalization-group theory [6–11]. It has been shown that the surface Curie temperature can be higher than that of bulk when the exchange interaction at the surface is larger than a critical value, and that the critical exponents of surface magnetization can be different from those of the bulk magnetization.

With depth-averaged experimental techniques, however, direct verification of the noncollinear magnetic structure and depth-dependent phase transition near surfaces and interfaces is difficult. The noncollinear magnetic structure has been suggested to exist for magnetic thin films by obtaining depth-dependent information on the magnetization with polarized neutron reflectometry, soft-x-ray resonant magnetic reflectivity [12], x-ray magnetic circular dichroism [13], and nuclear resonant scattering (NRS) [14–17]. While the magnetic reflectivity curve allows for analysis of the depth-dependent magnetic structure, the probing depth can be controlled by changing the takeoff angle or incident angle of the electrons or x rays.

In a recent study, we investigated the magnetization of Fe films with NRS of x rays in a glancing incidence condition to show that magnetization cants at the surface of an iron film [15]. In the present paper, we further explore more direct depth-resolved analysis of the magnetic structures of Fe films by growing films δ-doped with ^{57}Fe [18,19] on MgO(001) and Al_2O_3(0001) substrates with NRS of the synchrotron radiation (SR). The hyperfine structure of the ^{57}Fe nucleus can be measured as quantum beats in the time spectrum of x-ray scattering associated with nuclear resonant excitation [20–22]. Since the SR is linearly polarized, furthermore, the selection rule for Δm (m is the magnetic quantum number) limits the possible transitions depending on the polarization direction with respect to the magnetization direction, which allows us to distinguish the magnetization direction of samples [23–25]. Bulk Fe has an axis of easy magnetization in the $\langle 100 \rangle$ direction. On MgO(001), Fe(001) grows and has a perpendicular magnetization with respect to the surface [26–29]. On Al_2O_3(0001), on the other hand, Fe(110) grows, which is the hard axis of the magnetization. The magnetism of the Fe films was investigated by fabricating Fe films δ-doped with ^{57}Fe. By taking advantage of the ^{57}Fe-isotope-selective NRS, the magnetization direction and its temperature dependence were investigated in a depth-resolved way, and the magnetic structure was clarified with the aid of theoretical analysis.

*kawauchi@iis.u-tokyo.ac.jp

†fukutani@iis.u-tokyo.ac.jp

 ©2017 American Physical Society

TABLE I. Relation between the beat frequency and configuration.

Configuration	Main freq. (MHz)
$B_{hf} \perp H_{SR}$ and $B_{hf} \perp k_{SR}$	124, 72
$B_{hf} \parallel H_{SR}$ and $B_{hf} \perp k_{SR}$	72
$B_{hf} \perp H_{SR}$ and $B_{hf} \parallel k_{SR}$	72

II. EXPERIMENTAL AND THEORETICAL METHODS

The magnetization of Fe films was investigated by means of NRS of x rays at 14.4 keV [20–22], where ^{57}Fe nuclei in the sample are resonantly excited from the ground state to the first-excited state via the magnetic dipole transition, which is known as the Mössbauer effect [30,31]. The internal magnetic field of Fe was analyzed by the quantum beats observed in the time spectrum of the scattered x ray. The quantum beat frequency corresponds to the energy difference of the Zeeman-split nuclear levels. Since the SR is linearly polarized, the direction of the internal magnetic field B_{hf} at the ^{57}Fe nucleus site can be analyzed on the basis of the selection rule for the transition [25]. With the magnetic polarization H_{SR} and the wave vector k_{SR} of the incident x ray, the beat frequency depends on the relative direction of B_{hf} with respect to H_{SR} and k_{SR} as shown in Table I, which is evaluated with the internal magnetic field of 33 T for α-Fe.

The NRS experiments were *ex situ* performed at the PF AR-NE1A beamline in the High Energy Accelerator Research Organization (KEK, Japan). The SR was incident to the sample surface in a glancing condition with H_{SR} perpendicular to the sample surface, and the x ray scattered in the specular direction was detected with avalanche photodiodes in a time-resolved manner. After transferring the samples from the preparation chamber to the beamline through air, the azimuthal scans at room temperature were conducted in air, whereas the temperature dependence was measured in a vacuum chamber set at the beamline. The frequency of the quantum beat in the NRS time spectrum was analyzed using the maximum entropy method (MEM). The MEM is a powerful method to analyze the time spectrum with relaxation, and it has been applied successfully to the analysis of the nuclear magnetic resonance (NMR). It has been shown that a weak component in the frequency spectrum can be detected in NMR [32–36]. Since the relative intensity of the two beat components shown in Table I depends sensitively on the direction of B_{hf}, the direction and magnitude of the sample magnetization were evaluated by the analysis of the quantum beats. The relative amplitude of the two beat components obtained by MEM, on the other hand, tends to systematically deviate from the correct value. We have therefore evaluated such deviation by performing MEM analysis of the simulated time spectra, which is described in Appendix A.

The samples were prepared by depositing either of two Fe isotopes, namely ^{56}Fe enriched at 99.7% and ^{57}Fe enriched at 95.7%, on MgO(001) and Al_2O_3(0001) substrates at a substrate temperature of 430 K in an ultrahigh vacuum with a base pressure of 8×10^{-9} Pa. The substrates were heated at 573 K prior to Fe deposition, and the surface structure was confirmed to be 1×1 by RHEED. Two types of Fe films were fabricated on each substrate by alternately depositing ^{56}Fe and ^{57}Fe at deposition rates of 0.05–0.08 and 0.01 nm/s, respectively. The first type is the Interface sample, where a 1-nm-thick ^{57}Fe layer was initially deposited followed by deposition of a 20-nm-thick ^{56}Fe layer. The second type is the Middle sample, where 10-nm-thick ^{56}Fe, 1-nm-thick ^{57}Fe, and 10-nm-thick ^{56}Fe were sequentially evaporated on the substrates. While the ^{57}Fe probing layer for NRS is at the interface between the substrates and films in the former samples, it is expected to be in the middle of the films in the latter. It is noted that both the Interface and Middle samples are magnetically the same, because the two isotopes are chemically identical.

As confirmed by RHEED after Fe deposition, Fe(001) was epitaxially grown on MgO(001) with its [100] direction along [110] of the substrate and Fe(110) was grown on Al_2O_3(0001), which are consistent with previous studies [37–39]. The mean lattice constants of both films were the same as that of bulk bcc Fe within the experimental accuracy of RHEED. By comparing the Laue spots in the RHEED patterns with the simulated ones, Fe(110) on Al_2O_3(0001) was found to have three crystallographically equivalent domains rotated by 60°, which is also consistent with previous studies [40,41]. From the x-ray reflectivity measurement, the surface roughness was estimated to be 2.6 and 2.4 nm for the Interface and Middle samples on MgO(001), respectively, and 0.8 and 1.3 nm for the Interface and Middle samples on Al_2O_3(0001), respectively.

The detailed magnetic structure of Fe/MgO(001) was examined by theoretical calculations. The interface magnetic anisotropy energy and the layer exchange stiffness constant were evaluated with first-principles density-functional calculations using the Vienna ab initio simulation package (VASP) [42–44]. In the calculations, wave functions were expanded in a plane-wave basis set, and the behaviors of core electrons were described by the projector augmented wave (PAW) potential [45,46]. For the exchange and correlation energy, we adopted the spin-polarized generalized gradient approximation (GGA) [47]. We constructed supercells of Fe/MgO(001) multilayers with 25 atomic layers of bcc-Fe and 5 atomic layers of MgO, where the in-plane lattice constant of the supercells is that of bcc Fe (2.833 Å) following the RHEED observation. To match the lattices of Fe and MgO, the MgO lattice was assumed to be contracted by 5.5% in-plane and expanded by 4.8% out-of-plane. The k-point integration was performed using a modified tetrahedron method with Blöchl corrections [48] with $24\times24\times1$ k points in the first Brillouin zone of each Fe/MgO(001) supercell. The Fe/MgO(001) interfacial structure was fully optimized by relaxing the atomic positions while changing the longitudinal size of the supercells.

III. RESULTS

Figure 1(a) shows the NRS intensity as a function of the glancing angle of the incident x ray measured for the Interface sample on MgO(001). The NRS intensity obtained by summing the delayed emission in the time spectrum shows a broad distribution extending from 4 to 12 mrad. This is in contrast to the result on a ^{57}Fe film showing a maximum at 3.8 mrad [49], which corresponds to the critical angle for total reflection at the Fe surface of the nonresonant x ray with an

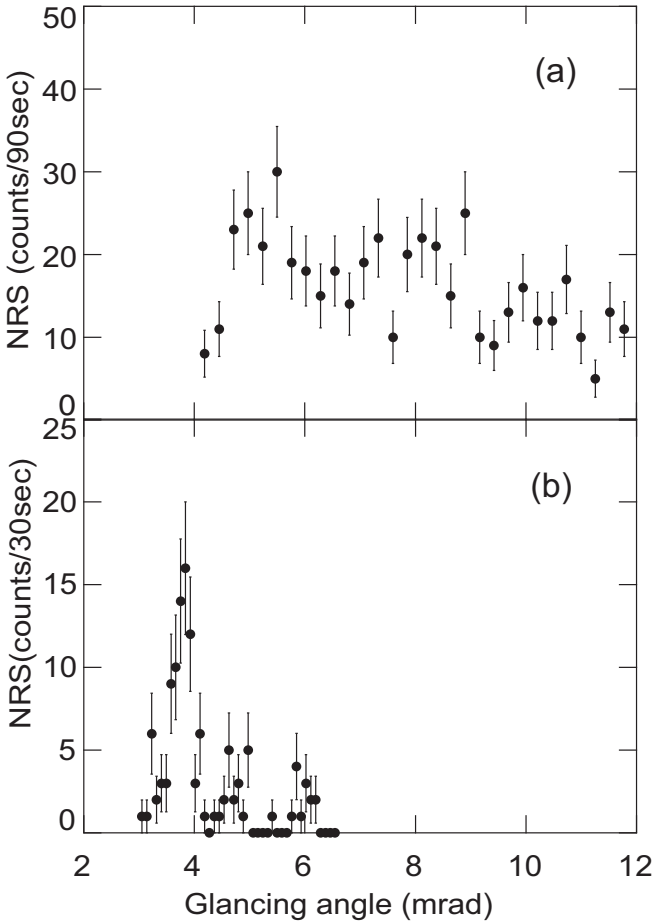

FIG. 1. Nuclear resonant scattering intensity of x rays as a function of the glancing angle taken for ^{56}Fe(20 nm)/^{57}Fe (1 nm)/MgO(001) (a) before and (b) after annealing at 773 K.

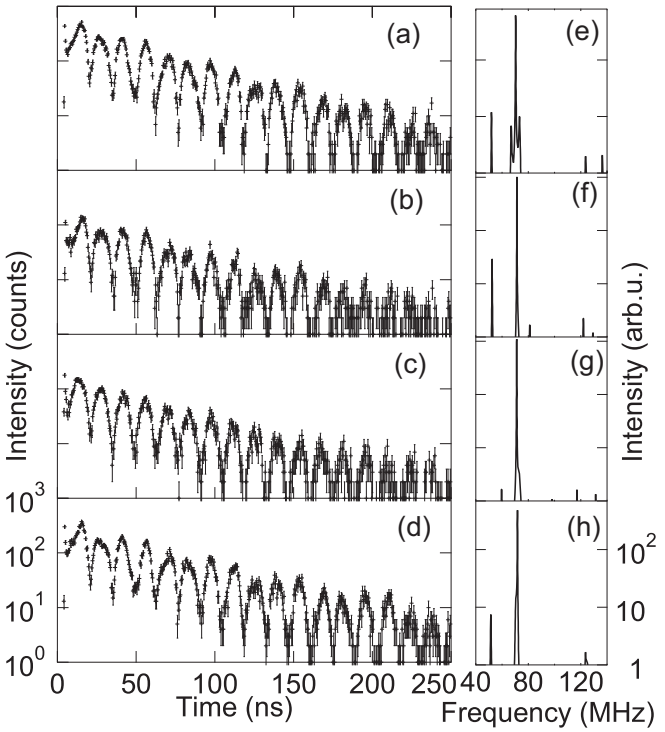

FIG. 2. Time spectra of the nuclear resonant scattering for ^{56}Fe/^{57}Fe/MgO(001) at a glancing angle of 5.2 mrad and azimuths of (a) MgO[1$\bar{1}$0], (b) MgO[010], (c) MgO[110], and (d) MgO[100]. The frequency spectra obtained for (a)–(d) by MEM are shown in (e)–(h), respectively.

energy of 14.4 keV. Since the penetration depth of the x ray at a glancing angle below 3.8 mrad is estimated to be about 2 nm [50], the ^{57}Fe layer at the interface is not detected below 3.8 mrad. At a glancing angle of larger than 4.0 mrad, on the other hand, the penetration depth of the x ray becomes larger than 20 nm, and the buried ^{57}Fe layer can be probed by NRS [49,51]. The NRS time spectra were therefore measured at a fixed glancing angle of larger than 4 mrad after confirming that sufficient scattering intensity is obtained.

Figure 2 shows the NRS time spectra taken at various azimuthal directions of the incident x ray for the Interface sample on MgO(001) and the results of the frequency analysis. All the time spectra reveal a clear oscillation corresponding to the quantum beat. As seen in the frequency spectra of Figs. 2(e)–2(h), a component of 72 MHz is dominant in all spectra, and the slight intensity at 144 MHz is ascribed to the harmonic component of 72 MHz, which is often observed in the MEM analysis. This quantum beat definitely indicates that the film is ferromagnetic α iron [52,53]. It is noted that the intensity of the 124 MHz component is less than 3% of the 72 MHz component independent of the azimuthal direction of the incident x ray. This implies that the magnetization direction at the interface of Fe/MgO(001) is mainly out-of-plane. If the magnetization were in-plane, a substantial intensity of the quantum beat with a frequency of 124 MHz would be observed at a certain azimuthal direction. Figure 3 shows the time spectra and their frequency spectra taken for the Middle sample on MgO(001). Whereas a single oscillation component is observed in Figs. 3(a) and 3(d), multiple oscillation components are obviously present in Fig. 3(c). The frequency spectra in Figs. 3(f) and 3(g) show the presence of two components at 124 and 72 MHz. The presence of the 124 MHz component definitely indicates that there is an in-plane magnetization component in the Middle sample on MgO(001).

From the intensities of the two components, the magnetization direction is estimated to be 72% out-of-plane at the interface and 97% in-plane at the middle of the film. These values correspond to mean magnetization directions of $58 \pm 8^\circ$ and $6 \pm 5^\circ$ with respect to the surface parallel direction at the interface and middle of the film, respectively. Note that the relative intensity of the two frequency components of 124 and 72 MHz changes depending on the azimuthal angle. This suggests that the in-plane magnetization is preferentially aligned in the Fe(100) direction rather than Fe(010) within the film plane. This uniaxial magnetization might be caused by the film growth condition, such as a residual magnetic field [16,37,38].

Figures 4 and 5 show the time spectra and their frequency spectra of the Interface and Middle samples on Al_2O_3(0001), respectively. As seen in the figures, the 124 MHz component appears in some specific directions for both Interface and Middle samples, which indicates the presence of the in-plane

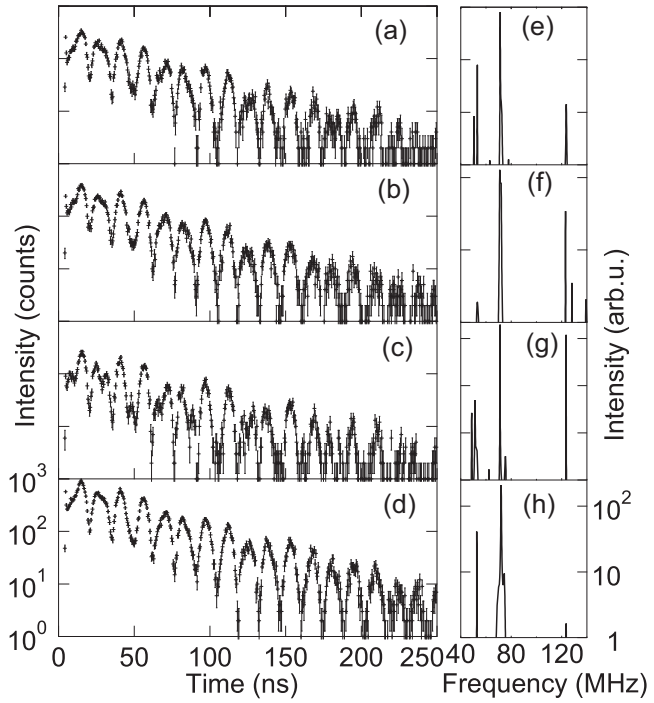

FIG. 3. Time spectra of the nuclear resonant scattering for ^{56}Fe/^{57}Fe/^{56}Fe/MgO(001) at a glancing angle of 5.8 mrad and azimuths of (a) MgO[1$\bar{1}$0], (b) MgO[010], (c) MgO[110], and (d) MgO[100]. The frequency spectra obtained for (a)–(d) by MEM are shown in (e)–(h), respectively.

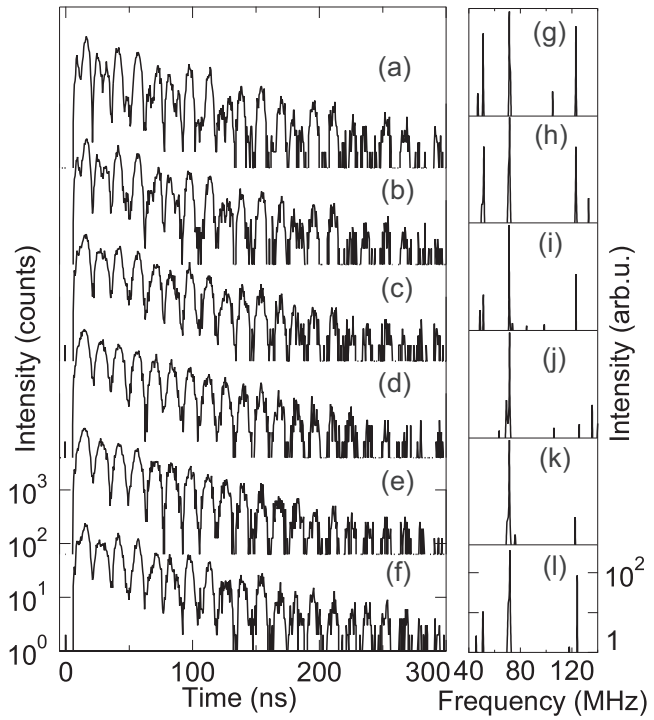

FIG. 4. Time spectra of the nuclear resonant scattering for ^{56}Fe/^{57}Fe/Al_2O_3(0001) at a glancing angle of 6.2 mrad and azimuths of (a) Al_2O_3[$\bar{1}$010], (b) Al_2O_3[$\bar{2}$110], (c) Al_2O_3[$\bar{1}$100], (d) Al_2O_3[$\bar{1}2\bar{1}0$], (e) Al_2O_3[01$\bar{1}$0], and (f) Al_2O_3[11$\bar{2}$0]. The frequency spectra obtained for (a)–(f) by MEM are shown in (g)–(l), respectively.

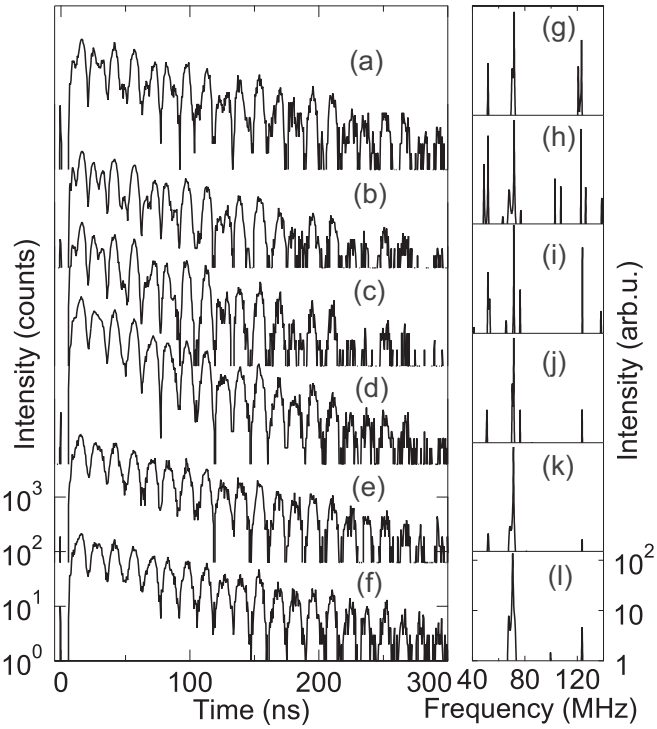

FIG. 5. Time spectra of the nuclear resonant scattering for ^{56}Fe/^{57}Fe/^{56}Fe/Al_2O_3(0001) at a glancing angle of 4.1 mrad and azimuths of (a) Al_2O_3[$\bar{1}$010], (b) Al_2O_3[$\bar{2}$110], (c) Al_2O_3[$\bar{1}$100], (d) Al_2O_3[$\bar{1}2\bar{1}0$], (e) Al_2O_3[01$\bar{1}$0], and (f) Al_2O_3[11$\bar{2}$0]. The frequency spectra obtained for (a)–(f) by MEM are shown in (g)–(l), respectively.

magnetization in both samples. From the relative intensities of the 124 and 72 MHz components, the magnetization direction is analyzed to be 82% in-plane at the interface and 83% in-plane at the middle of the film. These values correspond to mean magnetization directions of $25 \pm 6^\circ$ and $24 \pm 6^\circ$ with respect to the surface parallel direction. Although the cause for the inclined magnetization is not clear, the result is consistent with previous studies showing the presence of the perpendicular magnetization component [54,55]. Similarly to the results of Fig. 3, there is a variation in the intensity of the 124 MHz component depending on the azimuthal angle. This indicates that the in-plane magnetization mainly points to the Al_2O_3[$\bar{1}$010] and Al_2O_3[$\bar{2}$110] directions for the Interface and Middle samples, respectively.

Next, the temperature dependence of the NRS time spectrum was measured for the four samples. Figures 1(a) and 1(b) show the NRS intensity as a function of the glancing angle measured for the Interface sample on MgO(001) before and after annealing at 773 K, respectively. While the NRS intensity has a broad distribution extending from 4 to 12 mrad before annealing, a sharp maximum is observed at a glancing angle of 3.8 mrad after annealing. In a previous study on a thin ^{57}Fe film with a thickness of 24 nm, it is shown that the NRS intensity is sharply peaked at 3.8 mrad corresponding to the critical angle for total reflection of x rays at 14.4 keV when there are sufficient ^{57}Fe atoms at the surface [49]. The result of Figs. 1(a) and 1(b) suggests that part of the ^{57}Fe layer that had initially existed at the interface diffused to the surface of the

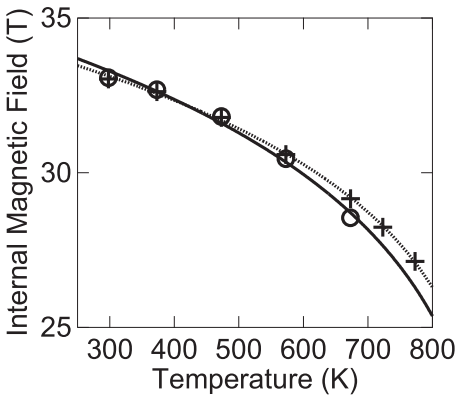

FIG. 6. Temperature dependence of the internal magnetic field B_{hf} taken for $^{56}Fe/^{57}Fe/MgO(001)$ (◯) at a glancing angle of 5.8 mrad and $^{56}Fe/^{57}Fe/^{56}Fe/MgO(001)$ (×) at a glancing angle of 6.1 mrad. Solid and dotted curves are fits of Eq. (2) with a common T_c value to the data of the former and latter samples, respectively. The obtained T_c is 903 K.

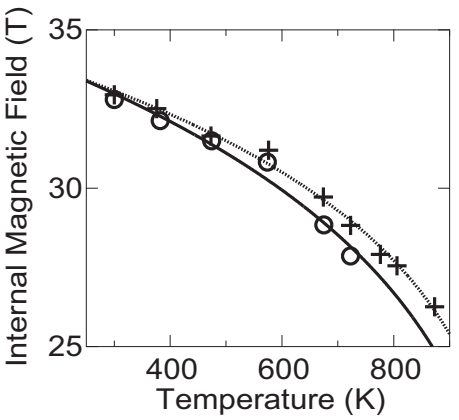

FIG. 7. Temperature dependence of the internal magnetic field B_{hf} taken for $^{56}Fe/^{57}Fe/Al_2O_3(0001)$ (◯) at a glancing angle of 6.1 mrad and $^{56}Fe/^{57}Fe/^{56}Fe/Al_2O_3(0001)$ (×) at a glancing angle of 5.8 mrad. Solid and dotted curves are fits of Eq. (2) with a common T_c value to the data of the former and latter samples, respectively. The obtained T_c is 1028 K.

Fe film after annealing at 773 K, where the nuclear-resonant x ray seems to undergo total reflection. In the present work, the glancing-angle dependence of the NRS intensity was measured for each sample at an elevated temperature to confirm that a sufficient NRS intensity was observed at a glancing angle higher than 4 mrad. As a result, the NRS time spectrum was measured up to temperatures of 673 and 773 K for the Interface samples on MgO(001) and $Al_2O_3(0001)$, respectively, and 773 and 883 K for the Middle samples on MgO(001) and $Al_2O_3(0001)$, respectively. Although we cannot recognize the atomic-level diffusion of ^{57}Fe during the measurements at elevated temperatures as observed in a previous study [19], we can exclude the possibility of complete ^{57}Fe diffusion in the entire film.

From the frequency analysis of the quantum beat in the time spectra, the internal magnetic field was evaluated for the Interface and Middle samples on MgO(001), which is plotted as a function of the sample temperature, as shown in Fig. 6. The internal magnetic fields decrease with increasing temperature. For the Interface and Middle samples on $Al_2O_3(0001)$, the internal magnetic fields also decrease as the sample temperature is raised, as shown in Fig. 7. For both substrates, the internal magnetic field for the Interface samples was found to be slightly smaller than that of the Middle samples.

IV. DISCUSSION

A. Magnetic structure

The experimental results of Figs. 2 and 3 indicate the mean magnetization direction is $58 \pm 8^\circ$ and $6 \pm 5^\circ$ with respect to the surface parallel direction at the interface and middle of the film, respectively. This suggests that the Fe film on MgO(001) has a noncollinear magnetic structure with the magnetization canted near the interface. On the other hand, the magnetic structure of the Fe film on $Al_2O_3(0001)$ is mainly aligned in the surface parallel direction. This difference might be due to the crystallographic direction of the Fe films, Fe(001) on MgO(001) and Fe(110) on $Al_2O_3(0001)$, and the interface chemical interaction. The Fe(001) surface has a perpendicular magnetocrystalline anisotropy (MCA) energy of 0.85 erg/cm^2 [56]. The Fe(110) surface, on the other hand, has a perpendicular MCA energy of 0.47 erg/cm^2, which is smaller than that of Fe(001). While the Fe(001) at the interface with MgO(001) intrinsically has a larger perpendicular anisotropy, the chemical interaction between Fe and O atoms at the interface further enhances the perpendicular anisotropy on MgO(001), as discussed below [26,56–58]. However, this chemical effect is expected to be smaller on $Al_2O_3(0001)$, because the topmost surface of $Al_2O_3(0001)$ is composed of Al atoms [59] and the Fe lattice does not match well with the substrate. While the interface has a perpendicular MCA, the shape anisotropy originating from the spin dipole interaction tends to make the magnetization in-plane. The magnetic structure of the Fe film is determined so that the total magnetic energy is minimized, and the Fe film on MgO(001) with a large MCA energy is considered to have a noncollinear magnetic structure, whereas that on $Al_2O_3(0001)$ with a small MCA energy is mainly aligned in the surface parallel direction.

In the following, we theoretically discuss the magnetic structure of the Fe film on MgO(001). We first estimate the interface MCA energy K_{int} of Fe/MgO(001) with first-principles calculations on the basis of the force theorem [60], i.e., the difference in the total energy for the magnetization oriented along the in-plane [100] and out-of-plane [001] directions, where the positive sign corresponds to the out-of-plane magnetization. After optimizing the structure, the Fe atoms at the interface are located above the O atoms with the Fe-O distance of 2.24 Å and the [100] of Fe aligned along [110] of MgO. The K_{int} value is evaluated to be 1.91 erg/cm^2 for Fe/MgO(001), which is consistent with a previous report [58]. Next, we estimate the interlayer exchange stiffness constant A of bcc Fe without the spin-orbit interaction. For the Fe(25 ML)/MgO(001) model, we fix the spin direction of the 12 layers near the interface, whereas those of the other 13 layers are forced to tilt by ϕ with respect to the 12 layers. Under this constrained magnetic structure, the total energy $E(\phi)$ relative to the collinear-spin structure ($\phi = 0$) was evaluated

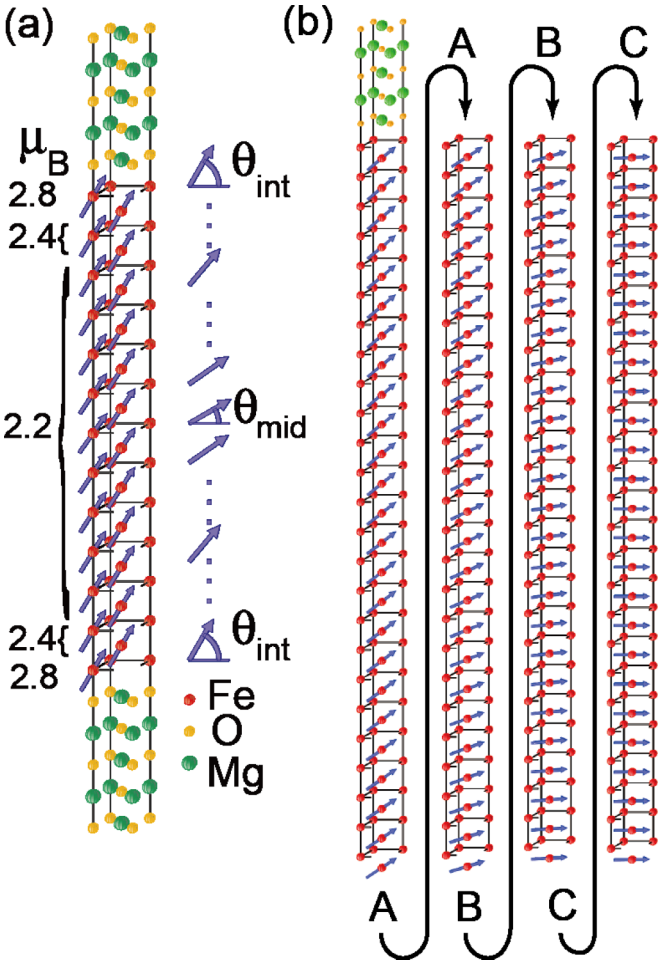

FIG. 8. (a) Schematic figure of the slab model for Fe/MgO(001) used in the first-principles density-functional calculations. The $\theta_{\rm int}$ and $\theta_{\rm mid}$ are the angles of the Fe spins with respect to the in-plane direction at the interface and the middle of the slab, respectively. The local magnetic moments are also shown in μ_B. (b) Schematic figure of the MgO/Fe(001) structure used in the model calculations expressed by Eq. (1). The structure contains five atomic layers of MgO and 200 atomic layers of Fe, where the characters A, B, and C at the bottom of the Fe layers denote the layers that are connected to those indicated by the same characters at the top. The spatial change of the local magnetization direction $\theta(z)$ of Fe atoms is shown for $W = 26$ nm and $\theta_{\rm int} = 40^\circ$ in Fig. 9.

by the self-consistent calculations. By fitting $A(1-\cos\phi)$ to the result of $E(\phi)$, we estimated the exchange stiffness constant A of the bcc Fe layer, which is consistent with a previous study [5]. In the present paper, we use the value of 2.41×10^{-6} erg/cm.

To clarify the magnetic structure in more detail, furthermore, we discuss the spatial change of the local magnetization direction. We consider a magnetic structure for 25 Fe layers shown in Fig. 8(a), where the Fe spin direction changes from $\theta_{\rm int}$ at the interface to $\theta_{\rm mid}$ at the middle of the film. Then, the spatial change of the local magnetization direction, $\theta(z)$, as a function of the distance z from the interface was determined by self-consistent calculations with the spin-orbit interaction. With $\theta_{\rm int} = 59.3^\circ$ and $\theta_{\rm mid} = 55^\circ$, it was found

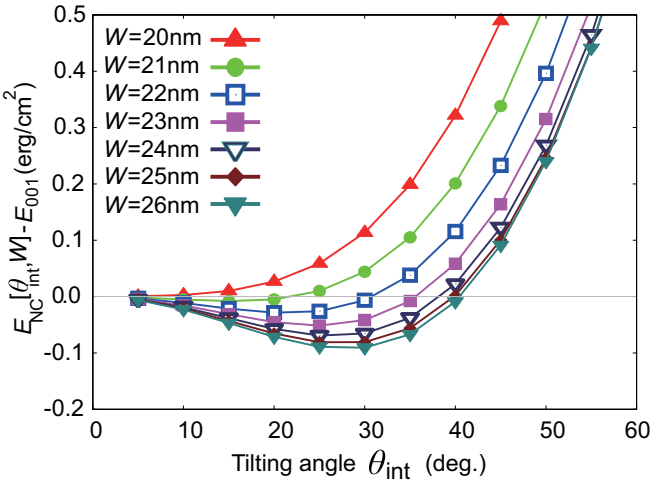

FIG. 9. Total energy of a noncollinear magnetic structure $E_{\rm NC}$ relative to the uniform magnetic structure in the perpendicular direction E_{001} as a function of $\theta_{\rm int}$ for various thicknesses W of the Fe films on MgO. The negative value indicates that the noncollinear magnetic structure is energetically more stable than that of the collinear one.

that $\theta(z)$ changes gradually from $\theta_{\rm int}$ to $\theta_{\rm mid}$, which is well described by the function of $\theta(z) = \theta_{\rm int}\cos^2(\pi z/2W)$ with a constant W, and that the total energy is smaller than that of a perpendicularly magnetized structure in the entire film. This means that the interfacial perpendicular MCA causes a noncollinear magnetic structure at the cost of the exchange energy due to the nonparallel configuration of the neighboring spins.

The total energy on the basis of the first-principles calculations, however, does not include the shape magnetic anisotropy originating from the magnetic dipole interaction. Thus, we consider a model structure for an Fe film with a thickness of $2W$ sandwiched by MgO, and we evaluate the stability of a noncollinear magnetic structure, where the magnetization direction $\theta(z)$ gradually changes from $\theta_{\rm int}$ at the interface to 0° at $z = W$ following the relation of $\theta(z) = \theta_{\rm int}\cos^2(\pi z/2W)$. By taking account of $K_{\rm int}$ at the Fe/MgO(001) interface, the exchange energy, and the shape magnetic anisotropy, the total magnetic energy $E_{\rm NC}$ is expressed as follows:

$$E_{\rm NC} = -K_{\rm int}\sin^2\theta_{\rm int} + \int_0^W \left[A\left(\frac{d\theta}{dz}\right)^2 + 2\pi M^2\sin^2\theta\right]dz, \tag{1}$$

where the first, second, and third terms represent the interface anisotropic energy, exchange energy, and the shape anisotropic energy with a magnetization M, respectively. The magnetic structure of the Fe film on MgO(001) can be determined by minimizing the total energy. By substituting 2.02×10^7 erg/cm^2 for $2\pi M^2$, the total magnetic energy with respect to that for the fully perpendicular magnetization of the entire film, E_{001}, is plotted as a function of W for various $\theta_{\rm int}$ values in Fig. 9. The calculation results show that the noncollinear magnetic structure is barely stable when $W \leqslant 20$ nm, because the exchange energy between neighboring spins becomes higher. When $W \geqslant 21$ nm, on the other hand, the noncollinear magnetic structure is energetically more stable

than the collinear one at $\theta_{\rm int} \leqslant 40^\circ$. This is roughly consistent with the present experimental result.

B. Phase transition

The internal magnetic field $B_{\rm hf}$ evaluated by the NRS experiment can be regarded as an order parameter for the magnetic phase transition [61,62]. With increasing temperature, the internal magnetic field gradually decreases and eventually becomes zero at the Curie temperature, T_c. The order parameter is expressed in a high-temperature region with the critical exponent β as [63]

$$B_{\rm hf}(T) = B_{\rm hf}(0)\left(1 - \frac{T}{T_c}\right)^{\beta}. \quad (2)$$

Although the number of data is limited due to the self-diffusion of Fe atoms, the internal magnetic field at the interface is smaller than those at the middle of the films, as shown in Figs. 6 and 7, which suggests the magnetic transition at the interface starts at a lower temperature. This is intuitively reasonable considering that the Fe atom at the interface has a lower number of coordination as compared to those of the bulk. Two possible interpretations can be conceived for the cause, namely an enhanced critical exponent and lowered Curie temperature at the interface. Note that the data points are rather far from T_c. Although evaluation of the critical exponent on the basis of these data is difficult, we tentatively analyze the present data with Eq. (2).

The temperature dependence of the order parameter for the magnetic phase transition of magnetic materials with free surfaces was theoretically studied in detail [6–11]. An important parameter is the exchange interaction energy J_s at a surface. When J_s is larger than a critical value of about $1.5J$, where J is the bulk exchange interaction, the surface magnetization remains above bulk T_c. When J_s is smaller than the critical value, the critical exponent of the surface magnetization becomes larger than the bulk value. It was shown that the surface β is about 0.8 and becomes smaller as J_s/J approaches the critical value [6–11]. A previous spin-resolved photoemission study on Fe(001) has shown that the surface exponent is larger than the bulk value [64]. As the translational symmetry is lost at interfaces as well as surfaces, the theory may be applied to the interface magnetism.

According to the first-principles calculations, the magnetic moment at the interface is $2.8\mu_B$, which is larger than the value of $2.2\mu_B$ at the middle of the film, as shown in Fig. 8(a). By taking into account the exchange stiffness ratio at the interface and middle of the film, the exchange interaction ratio J_s/J is estimated at 1.18, which is clearly smaller than the critical value of $\sim$1.6 evaluated in theoretical studies [8,9]. The present data of Fig. 6 show that the interface magnetization is smaller than that at the middle of the film, which is consistent with the calculation result that the J_s/J is smaller than the critical value. By assuming the transition temperature is the same for both the interface and middle of the films, Eq. (2) was fitted to the experimental data, which are shown by solid and dotted curves in Figs. 6 and 7. The obtained critical exponent β was 0.152 ± 0.009 and 0.130 ± 0.009 for the Interface and Middle samples, respectively, on MgO(001) with T_c of 903 K. Those on Al_2O_3(0001) were 0.182 ± 0.001 and 0.152 ± 0.002 for the Interface and Middle samples, respectively, with T_c of 1028 K. The β value at the interface seems to be larger than that at the middle of the sample, which is qualitatively consistent with the theoretical results. It is noted that the values of β's of all samples are close to 1/8, which corresponds to the 2D Ising model as observed in ultrathin Fe films [65,66] in contrast to the bulk experimental value of 0.34 [67,68].

We finally comment on the other possibility that T_c at the interface is lower than that at the middle of the film. Previous theoretical studies showed that the surface T_c can be higher than that of bulk when the exchange interaction at the surface is larger than a critical value. In contrast to this, surface T_c is the same as that of bulk when the surface exchange interaction is smaller than the critical value [7–11]. In the solid-liquid phase transition, on the other hand, it is known that surface melting occurs in a certain condition [69,70]. Surface melting is a phenomenon that the atoms at the surface of a solid melts before the entire solid melts. This indicates that the melting temperature at the surface is lower than that of bulk. From the analogy of the magnetic system with the solid-liquid system, the Curie temperature of the magnetic phase transition may well be lower at surfaces or interfaces when the exchange interaction is weaker at surfaces or interfaces. We tentatively fit Eq. (2) to the experimental data for the Fe film on Al_2O_3(0001) without fixing T_c, and we obtained T_c of 857 ± 38 and 1028 ± 50 K for the Interface and Middle samples, respectively, with β of 0.12 ± 0.01 and 0.15 ± 0.02. It seems that T_c at the interface is lower than that at the middle of the film.

Although we cannot reach a definite conclusion, the interface magnetization behaves differently than the middle of the film, which could be further confirmed by theoretical analysis with a method such as the Gaussian kernel regression method [71].

V. CONCLUSION

The magnetic structure of Fe thin films with a thickness of 20 nm grown on MgO(001) and Al_2O_3(0001) surfaces was investigated by means of nuclear resonant scattering of linearly polarized x-ray and theoretical calculations with the aid of first-principles calculations. On MgO(001), the magnetization was found to be dominantly out-of-plane at the interface and in-plane at the middle of the film, indicating that the Fe film has a noncollinear magnetic structure. On Al_2O_3(0001), on the other hand, the magnetization was mainly in-plane in the entire film. By evaluating the interface magnetocrystalline anisotropy energy and exchange stiffness constant with first-principles calculations, the noncollinear magnetic structure was shown to be energetically more stable than the collinear structure. The temperature dependence of the internal magnetic field was also examined in a depth-resolved way. The experimental data suggest that the internal magnetic field at the interface is smaller than that of the middle of the film on both substrates, suggesting that the magnetic phase transition starts at the interface at a lower temperature than the entire film.

ACKNOWLEDGMENTS

We thank N. Hatano and T. Nakamura for valuable discussion on the magnetic phase transition. This work was

performed with the approval by the Institute of Materials Structure Science, High Energy Accelerator Research Organization (KEK) as a proposal number of 2010G188, 2012G603, 2014G577. This research was supported by Grants-in-Aid for Scientific Research (Grants No. 24760026, No. 24246013, and No. 26108705) of the Japan Society for the Promotion of Science (JSPS).

APPENDIX: ANALYSIS OF THE POLARIZATION-DEPENDENT NRS TIME SPECTRUM

For the analysis of the magnetization direction on the basis of the NRS selection rule, the quantum beat components of the NRS spectrum need to be quantitatively analyzed. The relative amplitudes of multiple quantum beats obtained with the maximum entropy method (MEM), however, often depend on the data acquisition condition, such as the time window. We therefore constructed the NRS time spectra with various amplitude ratios, and we performed the MEM analysis under the condition corresponding to the present experiment. In the magnetic dipole transition of a ^{57}Fe nucleus with m_g and m_e the magnetic quantum numbers of the ground and first-excited states, respectively, there are six allowed transitions with $m_g = +1/2 \rightarrow m_e = (+3/2, +1/2, -1/2)$ and $m_g = -1/2 \rightarrow m_e = (+1/2, -1/2, -3/2)$, each of which in the parentheses corresponds to the $\Delta m = +1$, 0, and -1 transition. The transition energies are denoted by $\hbar\omega_1, \ldots, \hbar\omega_6$ in order of descending energy. When these transitions are coherently induced with equal amplitudes, depending on Δm, the x-ray wave functions, $\tilde{F}_{\Delta m}(t)$, are classified into

$$\begin{aligned}\tilde{F}_{+1}(t) &= (a_1 e^{i\omega_1 t} + a_3 e^{i\omega_3 t})e^{-t/2\tau},\\ \tilde{F}_{0}(t) &= (a_2 e^{i\omega_2 t} + a_5 e^{i\omega_5 t})e^{-t/2\tau},\\ \tilde{F}_{-1}(t) &= (a_4 e^{i\omega_4 t} + a_6 e^{i\omega_6 t})e^{-t/2\tau},\end{aligned} \tag{A1}$$

where $a_1, \ldots, a_6$ are the factors depending on the Clebsch-Gordan coefficients, and τ (141 ns) is the lifetime of the exited state of the ^{57}Fe nucleus [53]. The term due to the dynamical effect of the nuclear resonant scattering [72] is neglected in the present analysis because the oscillation due to the dynamical effect was not observed, and only a slight speedup induced by the dynamical effect was observed in the present experiment [72]. The interference between these wave functions yields quantum beats in the time spectrum. Depending on the relative configuration of $B_{\rm hf}$, $H_{\rm SR}$, and $k_{\rm SR}$, the scattered x-ray intensity is expressed as shown in Table II [53].

By defining the direction of $B_{\rm hf}$ by the polar coordinate (θ, ϕ) with $k_{\rm SR}$ and $H_{\rm SR}$ in the x and z directions in the Cartesian coordinate, the time spectrum is described as

$$I(t) = I_1(t)\sin^2\theta\sin^2\phi + I_2(t)\cos^2\theta + I_3(t)\sin^2\theta\cos^2\phi. \tag{A2}$$

In the case of ferromagnetic α-Fe with an internal magnetic field of 33 T, the main frequencies of cases 1, 2, and 3 in Table II are 124, 72, and 72 MHz, respectively [52]. Since the 124 MHz component is included only in $I_1(t)$, the direction of $B_{\rm hf}$ can be evaluated from the intensity ratio of the 124 and 72 MHz components, R. When ϕ is changed, R takes a minimum and a maximum at $\phi = 0$ and $\pi/2$, respectively.

To evaluate the R value from the experimental NRS time spectrum, we constructed the NRS time spectrum on the basis of Eq. (A2) and conducted the MEM frequency analysis at various θ's and ϕ's. The obtained result at $\phi = \pi/2$ is plotted as a function of θ in Fig. 10, which shows a nonlinear relation. Figure 11, on the other hand, shows the R value as a function of ϕ at $\theta = \pi/2$. The solid curves in the figures are fits with a polynomial function, and by using these relations the direction of $B_{\rm hf}$ was estimated from the experimental intensity ratio of the 124 and 72 MHz components.

TABLE II. NRS intensity at three magnetization configurations.

Configuration	NRS intensity $I(t)$
$B_{\rm hf} \perp H_{\rm SR}$ and $B_{\rm hf} \perp k_{\rm SR}$	$I_1(t) = \lvert\tilde{F}_{+1}(t) + \tilde{F}_{-1}(t)\rvert^2$
$B_{\rm hf} \parallel H_{\rm SR}$ and $B_{\rm hf} \perp k_{\rm SR}$	$I_2(t) = 4\lvert\tilde{F}_{0}(t)\rvert^2$
$B_{\rm hf} \perp H_{\rm SR}$ and $B_{\rm hf} \parallel k_{\rm SR}$	$I_3(t) = 2 \mid \tilde{F}_{+1}(t) \mid^2 + 2 \mid \tilde{F}_{-1}(t) \mid^2$

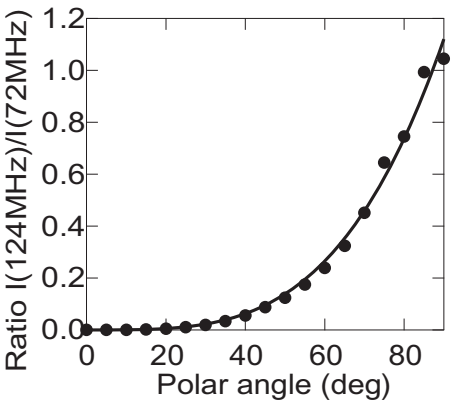

FIG. 10. Intensity ratio of the 124 and 72 MHz components at $\phi = \pi/2$ as a function of the polar angle of $B_{\rm hf}$ obtained by the MEM analysis of the simulated NRS time spectrum.

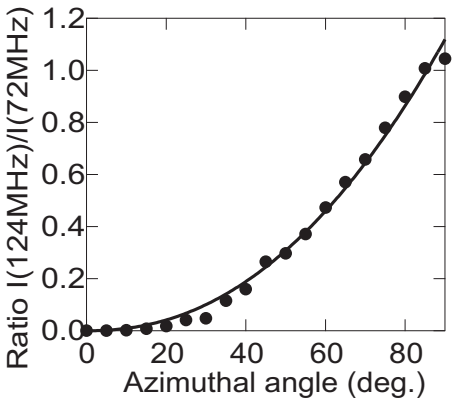

FIG. 11. Intensity ratio of the 124 and 72 MHz components at $\theta = \pi/2$ as a function of the azimuthal angle of $B_{\rm hf}$ obtained by the MEM analysis of the simulated NRS time spectrum.

[1] D. Suess, J. Lee, J. Fidler, and T. Schrefl, J. Magn. Magn. Mater. **321**, 545 (2009).
[2] P. Jensen and K. Bennemann, Surf. Sci. Rep. **61**, 129 (2006).
[3] J. M. D. Coey, Can J. Phys. **65**, 1210 (1987).
[4] D. L. Mills, Phys. Rev. B **39**, 12306 (1989).
[5] R. C. O'Handley and J. P. Woods, Phys. Rev. B **42**, 6568 (1990).
[6] U. Gradmann, J. Magn. Magn. Mater. **100**, 481 (1991).
[7] D. L. Mills, Phys. Rev. B **3**, 3887 (1971).
[8] K. Binder and P. C. Hohenberg, Phys. Rev. B **9**, 2194 (1974).
[9] K. Binder and D. P. Landau, Phys. Rev. Lett. **52**, 318 (1984).
[10] K. Ohno, Y. Okabe, and A. Morita, Prog. Theor. Phys. **71**, 714 (1984).
[11] H. W. Diehl and E. Eisenriegler, Phys. Rev. B **30**, 300 (1984).
[12] E. Jal, M. Dabrowski, J. M. Tonnerre, M. Przybylski, S. Grenier, N. Jaouen, and J. Kirschner, Phys. Rev. B **91**, 214418 (2015).
[13] K. Amemiya, M. Sakamaki, M. Mizusawa, and M. Takeda, Phys. Rev. B **89**, 054404 (2014).
[14] R. Röhlsberger, H. Thomas, K. Schlage, E. Burkel, O. Leupold, and R. Rüffer, Phys. Rev. Lett. **89**, 237201 (2002).
[15] T. Kawauchi, K. Fukutani, M. Matsumoto, K. Oda, T. Okano, X. W. Zhang, S. Kishimoto, and Y. Yoda, Phys. Rev. B **84**, 020415 (2011).
[16] T. Ślęzak, M. Zając, M. Ślęzak, K. Matlak, A. Kozioł-Rachwał, D. Wilgocka-Ślęzak, A. I. Chumakov, R. Rüffer, and J. Korecki, Phys. Rev. B **87**, 094423 (2013).
[17] T. Ślęzak, M. Ślęzak, M. Zając, K. Freindl, A. Kozioł-Rachwał, K. Matlak, N. Spiridis, D. Wilgocka-Ślęzak, E. Partyka-Jankowska, M. Rennhofer, A. I. Chumakov, S. Stankov, R. Rüffer, and J. Korecki, Phys. Rev. Lett. **105**, 027206 (2010).
[18] J. Tyson, A. H. Owens, J. C. Walker, and G. Bayreuther, J. Appl. Phys. **52**, 2487 (1981).
[19] J. Korecki and U. Gradmann, Phys. Rev. Lett. **55**, 2491 (1985).
[20] E. Gerdau, R. Rüffer, R. Hollatz, and J. P. Hannon, Phys. Rev. Lett. **57**, 1141 (1986).
[21] R. Röhlsberger, Hyperfine Interact. **123**, 455 (1999).
[22] J. Hannon and G. Trammell, Physica B **159**, 161 (1989).
[23] H. Frauenfelder, D. E. Nagle, R. D. Taylor, D. R. F. Cochran, and W. M. Visscher, Phys. Rev. **126**, 1065 (1962).
[24] R. Nussbaum and R. Housley, Nucl. Phys. **68**, 145 (1965).
[25] G. Smirnov, Hyperfine Interact. **123**, 31 (1999).
[26] H. X. Yang, M. Chshiev, B. Dieny, J. H. Lee, A. Manchon, and K. H. Shin, Phys. Rev. B **84**, 054401 (2011).
[27] J. W. Koo, S. Mitani, T. T. Sasaki, H. Sukegawa, Z. C. Wen, T. Ohkubo, T. Niizeki, K. Inomata, and K. Hono, Appl. Phys. Lett. **103**, 192401 (2013).
[28] T. Maruyama, Y. Shiota, T. Nozaki, K. Ohta, N. Toda, M. Mizuguchi, A. A. Tulapurkar, T. Shinjo, M. Shiraishi, S. Mizukami, Y. Ando, and Y. Suzuki, Nat. Nanotechnol. **4**, 158 (2009).
[29] J. Balogh, I. Dézsi, C. Fetzer, J. Korecki, A. Kozoł-Rachwał, E. Młyńczak, and A. Nakanishi, Phys. Rev. B **87**, 174415 (2013).
[30] R. L. Mössbauer, Z. Phys. **151**, 124 (1958).
[31] K. Ono, A. Ito, and E. Hirahara, J. Phys. Soc. Jpn. **17**, 1615 (1962).
[32] J. A. Jones and P. J. Hore, J. Magn. Reson. **92**, 276 (1991).
[33] E. D. Lade, J. Skilling, J. Staunton, S. Sibisi, and R. G. Brereton, J. Magn. Reson. **62**, 437 (1985).
[34] M. Sakata, T. Uno, and M. Takata, J. Appl. Cryst. **26**, 159 (1993).
[35] P. J. Hore, J. Magn. Reson. **62**, 561 (1985).
[36] J. F. Martin, J. Magn. Reson. **65**, 291 (1985).
[37] J. Costa-Kramer, J. Menendez, A. Cebollada, F. Briones, D. Garca, and A. Hernando, J. Magn. Magn. Mater. **210**, 341 (2000).
[38] H. Jaffres, L. Ressier, J. P. Peyrade, A. R. Fert, P. Gogol, A. Thiaville, A. Schuhl, and F. Nguyen Van Dau, J. Appl. Phys. **84**, 4375 (1998).
[39] E. Młyńczak, K. Freindl, N. Spiridis, and J. Korecki, J. Appl. Phys. **113**, 024320 (2013).
[40] C. Quintana, J. Menendez, Y. Huttel, M. Lancin, E. Navarro, and A. Cebollada, Thin Solid Films **434**, 228 (2003).
[41] Y. Shiratsuchi, Y. Endo, and M. Yamamoto, Sci. Technol. Adv. Mater. **5**, 73 (2004).
[42] G. Kresse and J. Hafner, Phys. Rev. B **47**, 558 (1993).
[43] G. Kresse and J. Furthmuller, Comput. Mater. Sci. **6**, 15 (1996).
[44] G. Kresse and J. Furthmüller, Phys. Rev. B **54**, 11169 (1996).
[45] P. E. Blöchl, Phys. Rev. B **50**, 17953 (1994).
[46] G. Kresse and D. Joubert, Phys. Rev. B **59**, 1758 (1999).
[47] J. P. Perdew, K. Burke, and M. Ernzerhof, Phys. Rev. Lett. **77**, 3865 (1996).
[48] P. E. Blöchl, O. Jepsen, and O. K. Andersen, Phys. Rev. B **49**, 16223 (1994).
[49] A. Q. R. Baron, J. Arthur, S. L. Ruby, A. I. Chumakov, G. V. Smirnov, and G. S. Brown, Phys. Rev. B **50**, 10354 (1994).
[50] J. P. Hannon, N. V. Hung, G. T. Trammell, E. Gerdau, M. Mueller, R. Rüffer, and H. Winkler, Phys. Rev. B **32**, 5068 (1985).
[51] J. P. Hannon, G. T. Trammell, M. Mueller, E. Gerdau, R. Rüffer, and H. Winkler, Phys. Rev. B **32**, 6363 (1985).
[52] C. E. Violet and D. N. Pipkorn, J. Appl. Phys. **42**, 4339 (1971).
[53] R. Röhlsberger, J. Bansmann, V. Senz, K. L. Jonas, A. Bettac, K. H. Meiwes-Broer, and O. Leupold, Phys. Rev. B **67**, 245412 (2003).
[54] O. Lenoble, J. Bobo, L. Kennet, H. Fischer, P. Bauer, and M. Piecuch, Thin Solid Films **275**, 64 (1996).
[55] K. Liu, D. Shen, J. Zhang, B. Li, X. Wu, Q. Feng, Y. Lu, and X. Fan, J. Magn. Magn. Mater. **303**, 79 (2006).
[56] Y. Miura, M. Tsujikawa, and M. Shirai, J. Appl. Phys. **113**, 233908 (2013).
[57] C.-G. Duan, J. P. Velev, R. F. Sabirianov, Z. Zhu, J. Chu, S. S. Jaswal, and E. Y. Tsymbal, Phys. Rev. Lett. **101**, 137201 (2008).
[58] M. K. Niranjan, C.-G. Duan, S. S. Jaswal, and E. Y. Tsymbal, Appl. Phys. Lett. **96**, 222504 (2010).
[59] J. Ahn and J. W. Rabalais, Surf. Sci. **388**, 121 (1997).
[60] M. Weinert, R. E. Watson, and J. W. Davenport, Phys. Rev. B **32**, 2115 (1985).
[61] A. R. Arends, C. Hohenemser, and R. M. Suter, Z. Phys. B **37**, 203 (1980).
[62] C. Hohenemser, T. Kachnowski, and T. K. Bergstresser, Phys. Rev. B **13**, 3154 (1976).
[63] M. E. Fisher, Rev. Mod. Phys. **46**, 597 (1974).
[64] E. Kisker, K. Schröder, W. Gudat, and M. Campagna, Phys. Rev. B **31**, 329 (1985).
[65] Z. Q. Qiu, J. Pearson, and S. D. Bader, Phys. Rev. B **49**, 8797 (1994).
[66] C. H. Back, C. Würsch, A. Vaterlaus, U. Ramsperger, U. Maier, and D. Pescia, Nature (London) **378**, 597 (1995).

[67] R. S. Preston, S. S. Hanna, and J. Heberle, Phys. Rev. **128**, 2207 (1962).
[68] L. P. Kadanoff, W. Götze, D. Hamblen, R. Hecht, E. A. S. Lewis, V. V. Palciauskas, M. Rayl, J. Swift, D. Aspnes, and J. Kane, Rev. Mod. Phys. **39**, 395 (1967).
[69] J. G. Dash, Contemp. Phys. **30**, 89 (1989).
[70] H. Lowen, Phys. Rep. **237**, 249 (1994).
[71] T. Nakamura, Phys. Rev. E **93**, 011301 (2016).
[72] G. V. Smirnov, Hyperfine Interact. **97**, 551 (1996).